

CHARACTERIZATION OF HIGH-DENSITY WC-CO BULK STRUCTURES FABRICATED BY SELECTIVE LASER MELTING

Avery Carroll, Rachel Carey, Michael Hurst, Michael Liu, Mathew Kuttolamadom¹
Texas A&M University
College Station, TX

ABSTRACT

The objective of this research is to evaluate the feasibility of using a high energy laser-based additive manufacturing process to fabricate tungsten-carbide-cobalt (WC-Co) bulk structures that have properties comparable to those achieved by traditional fabrication methods. In particular, this work will investigate the properties and performance of these hard carbides densified by sintering alone, as compared to methods (such as hot isostatic pressing (HIP) and spark plasma sintering (SPS)) which impart simultaneous compaction and sintering. For this, a design of experiments was utilized to investigate the pertinent process parameter design space for the selective laser melting (SLM) process with a view to manufacture structurally-integral samples. Besides organizing qualitative observations, the effects of these process conditions were correlated with the resulting physical properties (viz., density, micro-scale composite hardness, and nano-scale hardness and Young's modulus), as well as with microstructure and chemical compositions. Results showed certain samples with competitively-high densities, hardness and moduli, but with a large spread in properties, as is typical for such manufacturing processes; also, microstructural characteristics in line with desirable traits achievable via traditional methods was observed. Altogether, this work shows the promise of using SLM to fabricate bulk carbide structures.

Keywords: Density, WC-Co, Carbide, Selective laser melting.

NOMENCLATURE

d_f	laser focal spot diameter (μm)
E_v	volumetric energy density ($\frac{\text{J}}{\text{mm}^3}$)
h_s	hatch spacing, (mm)
HV	Vickers hardness
L	layer thickness (mm)
P	laser power (W)
v	scan speed ($\frac{\text{mm}}{\text{s}}$)

ρ_{rel} relative density (%)

1. INTRODUCTION

Tungsten carbide cobalt (WC-Co) is a cemented carbide with an excellent combination of mechanical properties, viz., high hardness and good toughness. Because of its high wear resistance, it is one of the most commonly used tooling materials in machining operations that span numerous industry sectors. Being a metal matrix composite, the tungsten carbide phase is the majority aggregate that imparts hardness, while the metallic cobalt binder is responsible for the good toughness of the composite. Accordingly, a higher percentage of WC typically increases the composite hardness, while the flexural strength (in bending) of such composites increases with Co content.

1.1 Fabrication of WC-Co

Being a cermet, WC-Co has a very high melting point, and hence it is impractical to fabricate bulk carbide structures via casting. Instead, various powder metallurgical techniques are typically used to combine carbide and binder (Co) particles by sequential or simultaneous compaction and sintering. Sintering is the bonding of particles into a coherent, predominantly solid structure by the application of heat to enable one or more mechanisms of atomic movement to the particle contact interface to occur [1], while compaction is the process of condensing powder by application of pressure. The compacting and sintering process developed by Schröter laid the foundation for production of cemented carbides [2], and its further development has enabled industrial carbide production with good control over its properties [3].

In its essential form, the desired ratio of WC and Co powders (typically, 1-20 wt.% of Co) is mixed mechanically, and the powder mixture subjected to compaction and sintering. If conducted sequentially, common compaction processes could involve either Magnetic Pulse Compaction (MPC), Equal Channel Angular Pressing (ECAP) or Rapid Omni Compaction

¹ Contact author: mathew@tamu.edu

(ROC) followed by a sintering technique such as Microwave sintering, Vacuum sintering or High frequency induction heated sintering. Instead, if a simultaneous compaction and sintering procedure is followed, Spark Plasma Sintering (SPS), Pulse Plasma Sintering (PPS) or Hot Isostatic Pressing (HIP) can be employed. Among these, HIP is one of the most commonly used commercial methods, and each process has its own merits and demerits in terms of minimal grain growth, densification, etc.

1.2 Additive Manufacturing of WC-Co

An additive manufacturing approach to fabricate WC-Co composites would be advantageous from geometry and property control perspectives, as is for other materials. However, the ceramic component (WC) of the composite imparts a high melting point, thus making the single step processing of the composite quite difficult. Consequently, multi-step additive manufacturing methods, such as binder jetting [4] has seen better successes. When considering high-energy laser based additive manufacturing processes such as selective laser melting (SLM) or laser engineered net shaping (LENS), the high melting point of the composite and the %Co content have been challenges. Another concern is the sintering/melting at atmospheric pressure conditions rather than at high pressures such as in HIP, SPS, etc. The absence of this compacting condition could result in lower densities (higher porosities). Never the less, a number of researchers have investigated the fabrication of WC-Co via such methods as detailed below.

Kumar et al. 2017 [5] used a 17% Co ratio to fabricate WC-Co via SLS at powers ranging from 270-370 W. They observed lowest porosity at 370 W (highest power) but least cracking at 270 W (lowest power). With scan speeds ranging from 900-1100 mm/s and 40 μm layer thickness and hatch spacing, this resulted in energy densities ranging from 40-237 J/mm^3 . With a preheated bed of 200 $^{\circ}\text{C}$, they observed the tradeoff between porosity vs. cracking based on powers. Further, lower scan speeds resulted in lowering cracking and increasing density. The study also reported a 5-7% evaporation in Co.

Khymrov et al. [6] used a 25% Co ratio to explore the process parameter design space to fabricate WC-Co via SLM. Testing out lower power ranges of 30-50 W, but at slower scan speeds of 10-100 mm/s, successful prints were obtained at 50 W and 100 mm/s. Lower powers yielded 'rougher' prints. The team extended their work in 2016 [7] to further test 50% and 75% Co ratios (very high) at 50-100 W powers and 10-100 mm/s scan speeds; the 50 W and 100 mm/s combination yielded the better structures. For the high Co content print (75%), no cracks were observed, however cracks were observed for the 50% Co print. Further in 2017 [8], the team tested Co ratios of 75%, 70%, 50% and 6% using the previously determined optimal scan speeds and laser powers of 100 mm/s and 50 W respectively, and reported on the microstructure and mechanical properties of the resulting prints, as well as qualitative observations on cracking.

Uhlmann et al. 2015 [9] fabricated 83-17% and 88-12% WC-Co composited via SLM with powers ranging between 40-380 W and scanning speeds ranging between 10-300 mm/s. Best results were observed for 100-200 W powers and 25-100 mm/s scan speeds. Further a high energy density of 1667 J/mm^3 resulted in high density but with cracking, while a lower energy density of 185 J/mm^3 resulted in lower density structures but with little cracking. The team further extended their work in 2018 [10] to explore the effects of vertical vs. horizontal builds. They found that the vertical build was better for heat distribution. Further, the high energy density (1500 J/mm^3) yielded high density, while the low energy density (350 J/mm^3) was better for obtaining higher transverse rupture strengths.

Additionally, Domeashenkov et al. 2018 [11] used a 12% Co ratio at 40 W power and scan speed of 130 mm/s to fabricate WC-Co. This study observed that the unstable thermal cycling during SLM made it difficult (due to unstable grain growth) to achieve close to theoretical densification without cracking. Chen et al. 2019 [12] used 80-20 % WC-Co powder to test a range of laser powers and scan speeds to span energy densities ranging from 200-285 J/mm^3 . This study concluded that the grain shape and size predominantly affected the microstructure of the prints, and that smaller spherical grain resulted in better builds. Other relevant studies include: the fabrication of WC-Co molds via SLS and infiltrating the structure with bronze to achieve better mechanical properties as well as wear resistance [13]; using a 17% Co ratio to fabricate WC-Co samples via SLS and moderate post heat treatment yielding better mechanical properties [14]; powder surface modification of WC by coating with stainless steel binder and subjected to SLS [15]; SLM of WC powder with an iron-based binder to achieve ~95% density [16].

The majority of the efforts so far have been centered on exploring process parameters for effective SLM of cemented carbides; however, the absence of a compaction step, the thermal cycling of the process and the spread in the resulting properties have been major challenges. This work aims to build on the literature to further push the process parameter design space for obtaining bulk structures using SLM, and to analyze the effects on the properties and performance of the structures.

2. MATERIALS AND METHODS

In this investigation, SLM via a Renishaw AM 400 machine was used to fabricate tungsten carbide cobalt specimens in the shape of inverted pyramids. The inverted pyramid configuration was used so that these specimens could be easily removed from the build plate, rather than by using the electric discharge machine (EDM); this would be an issue due to the low/non-conductivity of the cermet. One of the objectives of the research was to determine suitable process parameters to obtain dense WC-Co builds. There are many parameters that can be controlled during the SLM print including the laser power, laser scanning speed, hatch spacing, layer thickness, point distance, exposure time, etc. The relationship between the relevant SLM print parameters was determined by using the volumetric energy density (E_v) as:

$$E_v = \frac{P}{v \cdot h_s \cdot L} \quad (1)$$

The laser scanning speed (v) was determined by dividing the point distance by the exposure time at each point. The relation between the scan speed and the exposure time and point distance is given by:

$$v = \frac{x}{t} \quad (2)$$

The WC-Co powder was obtained from a commercial supplier with a composition of 83 wt.% WC and 17 wt.% Co; note that this Co % is higher than what is typically used in tooling used for machining (<10%). A higher %Co was intentionally chosen to avail the metallic binder's lower melting point (as compared to the WC ceramic phase) for potentially better fusion of the composite. The average particle size of the powder was 15-30 μm . The print was performed using a reduced build volume (RBV) setup within the SLM machine, and sixteen (16) WC-Co inverted pyramids (solid model in Figure 1) were printed on a stainless steel build plate. Some of the constant build parameters were 50 μm layer thickness, 40 μm point distance and 35 μm hatch spacing.

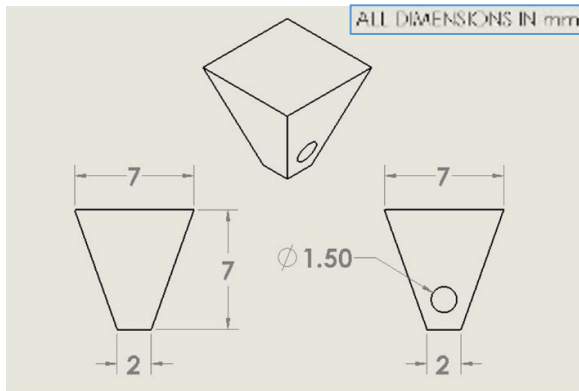


Figure 1: Dimensions of each specimen

Building on previous work from the literature, a design of experiments was formulated that varied the energy densities from 200-650 J/mm^3 , with powers ranging from 50-350 W and exposure times varying from 40-910 μs as shown in Table 1. The general procedure for this investigative study is as follows:

- Commercially obtained WC-17%Co powder was used in the Renishaw AM400 SLM machine's reduced build volume setup to print 16 inverted pyramids
- The sample densities were found using Archimedes principle, Torbal density kit and an analytical balance
- Samples were cut in the vertical/horizontal planes with a NTI Corporation high speed diamond cut-off saw
- An automatic mounting press was used to mount the samples in Bakelite
- Samples were polished manually with 400, 600 and 1200 grit polishing paper and then using an automatic polisher at 9, 6 and 1 μm

- Samples were analyzed using Wilson VH1102 Vickers hardness testing machine at HV 0.2 (kgf), scanning electron microscopy (SEM), energy-dispersive x-ray spectroscopy (EDS) and nano-indentation.

Table 1: Design of experiments for the study

Exposure Time (μs)	Power (W)				
	50	150	250	350	
Energy Density (J/mm^3)	200	280	93	56	40
	350	490	163	98	70
	500	700	233	140	100
	650	910	303	182	130

3. RESULTS

3.1 Observations from the Fabrication Process

To prepare the SLM machine, it was cleaned, vacuumed, the filters changed and the RBV assembled. The hopper was filled with the WC-Co powder and it was gently packed down and leveled before starting the print. The print was monitored and qualitative observations for each specimen noted.



Figure 2: Renishaw reduced build volume print in progress

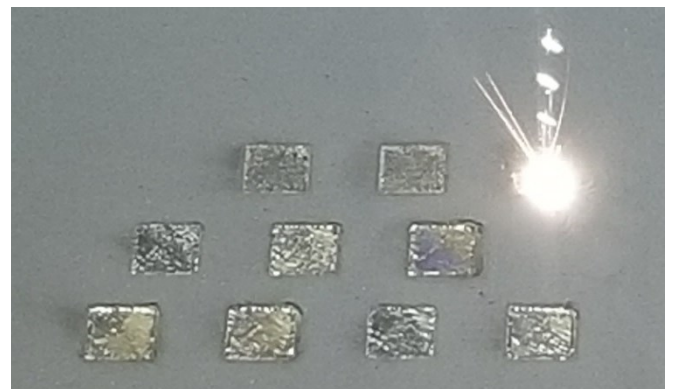


Figure 3: Close up view of the laser in action

The power flowability was very good, especially at the recommended grain sizes, and the wiper/coater was able to lay down smooth powder layers consistently. The prints completed without incident, and the build plate was extracted. The samples on the build plate (Figure 4) were carefully removed using pliers. Bluish discoloration and rough edges were observed in samples at the higher energy densities and/or high powers; the rest of them seemed to be of good quality with a grey smooth surfaces and sharp edges/corners.

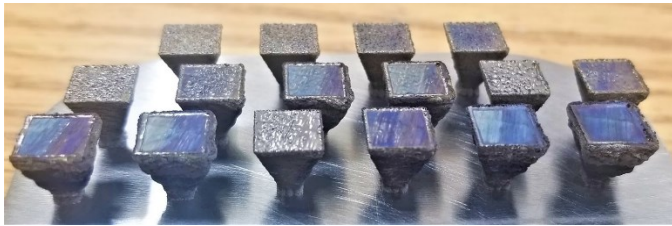


Figure 4: View of the completed specimens on build plate

3.2 Density

From among the different runs, the highest average density achieved was 13.99 g/cm^3 at a power of 150 W and an energy density of 650 J/mm^3 , which corresponds to a 96.73% relative density (row 1 of Table 2). As can be seen from this table, the relative density achieved was higher than some of the maximum densities reported in literature. Also note that our composite had a higher %Co content compared to the others. Since the density decreases with an increase in %Co (and relative %WC decrease [17]), this implies a competitively-high value for achieved density especially via SLM. It is also worth mentioning that the density reported in [6] are for nanostructured composites fabricated via SLM (smaller grain size, which suggests a higher hardness, as per Hall Petch equation), and that in [18] are for commercially fabricated materials (via HIP or other similar single-step methods).

Table 2: Densities at different %Co weight percentages

%wt. WC	%wt. Co	Theoretical Density (g/cm^3)	Achieved Density (g/cm^3)	Relative Density (%)
83	17	14.46	13.99	96.73
* 88	12	14.80	14.05	94.94
** 89	11	14.87	14.1	94.85

*row 2 - [18]; **row 3 - [6]

Error! Reference source not found. and Figure 6 show the effect of process parameters (exposure time, power, and volumetric energy density) on the relative and actual densities achieved. Density values generally increased with increasing exposure times (more input energy) at most laser powers. The 50 W samples generally resulted in lower sample densities regardless of exposure time or volumetric energy densities. With the exception of the 50 W samples, relative/actual densities were higher at the higher volumetric energy density of 650 J/mm^3 than the lowest 200 J/mm^3 . This suggests that there is a certain required minimum energy density needed for achieving high densities. However, a too high of an energy input might mean heat-based damage (bluish tinge, and frayed

or rough edges and surfaces). Also note the (expected) spread in properties due to a vast process-parameter design space being explored, in which certain conditions not optimal for making high-density samples.

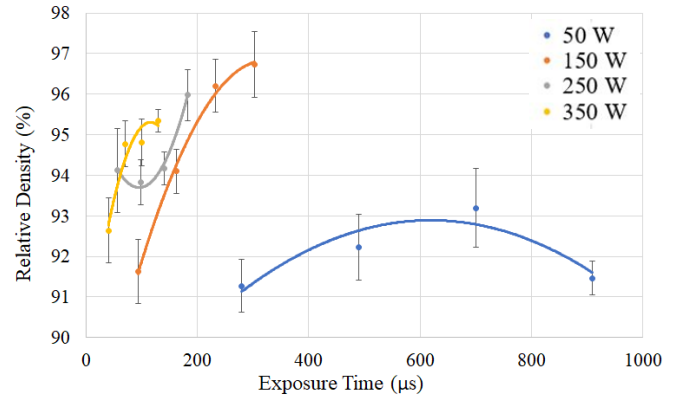


Figure 5: Effects of exposure time on relative density

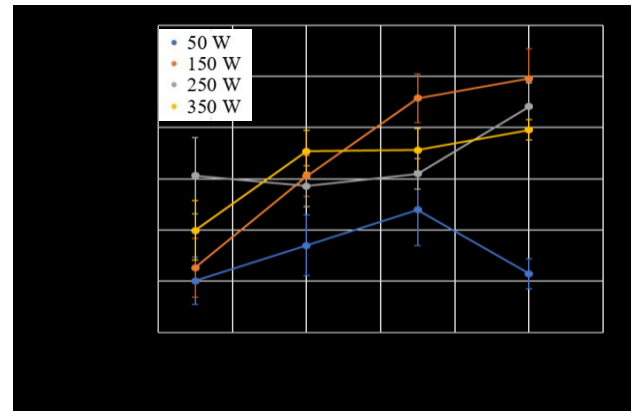


Figure 6: Effects of energy density on actual density

3.3 Composite Hardness

Due to the interder size, Vickers testing would end up probing both WC grains (harder) and the Co matrix (softer); hence the numbers reported would represent the composite hardness of the samples, rather than individual elements.

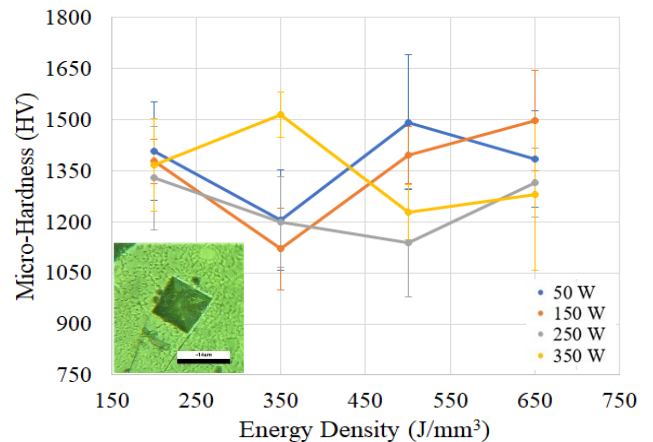


Figure 7: Vickers micro hardness numbers vs. energy densities

This spread in the hardness based on the area being probed is evident in Figure 7. With a laser power of 350 W and energy density of 350 J/mm³, the highest average hardness of 1513 HV was achieved, while the peak individual hardness of 1690 HV was measured at 50 W and 400 J/mm³. Literature reports 1550 HV for WC-6wt.%Co [19] fabricated via traditional methods such as HIP. Due to the higher Co content (17%) for this study, a lower composite hardness was expected, however the achieved comparable hardness of 1513 HV suggests the samples yielded competitively high hardness via SLM.

3.4 Nano-indentation Testing

Nano-indentation testing used a Berkovich tip having with 5 μm indenter and 200 mN indentation force. As shown in Figure 8 and Figure 9, the range of elastic modulus and hardness values had a significant spread that increased with energy density. In the case of elastic modulus, the number ranged from 33-620 GPa (literature reports about 560 GPa for the elastic modulus of the composite [20]). Similarly, nano-hardness also had a wide range, which suggests the individual probing of WC grains (harder) vs. the Co matrix (softer) vs. the WC-Co composite (intermediate hardness), all lying within the expected range of values for individual components such as WC and Co, as well as the composite (WC-Co) properties.

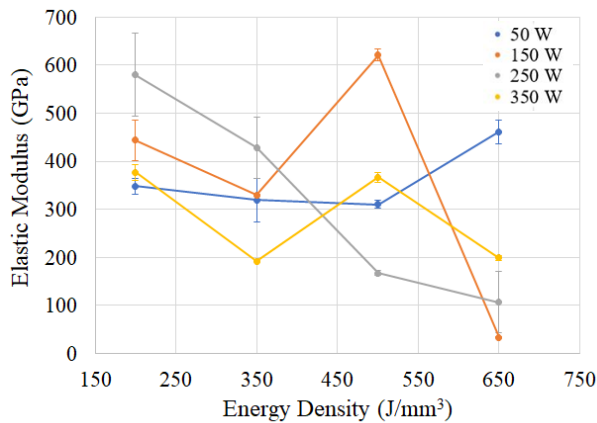


Figure 8: Elastic modulus vs. energy density & power

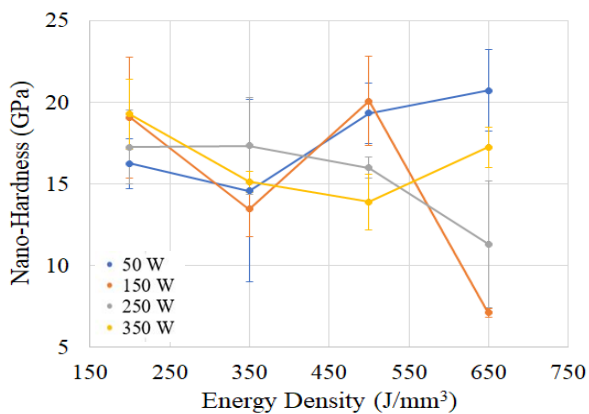


Figure 9: Hardness dependence on energy density & power

3.5 Microstructure

SEM was used to analyze the sample microstructures; a sampling is shown below. Figure 10(a) and (b) show the top as-printed surfaces of the 250 W–500 J/mm³ sample. Note the text indicators in the figures, highlighting relevant observations.

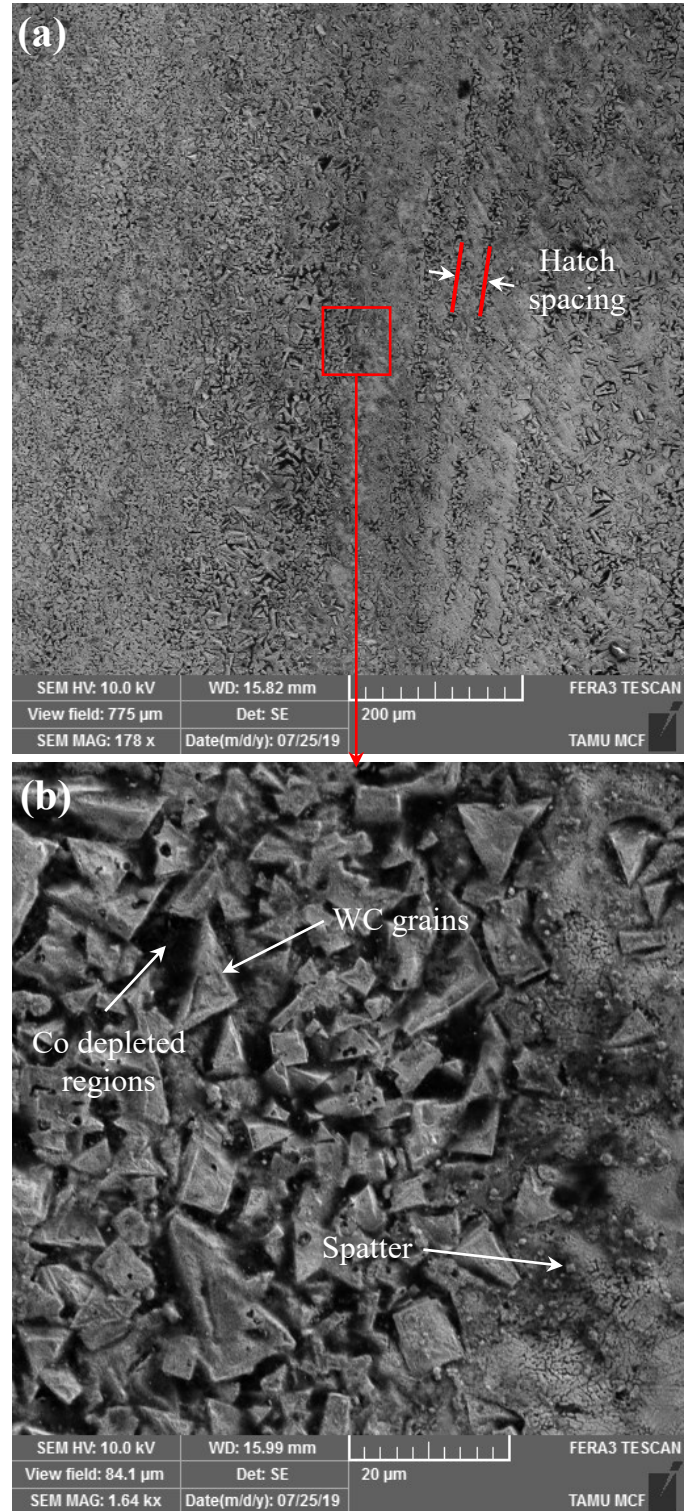


Figure 10: SEM images of as-printed top surface (unpolished)

A relatively rough surface was expected at the as-printed top layer of the samples, on which features matching the hatch spacing are visible along with minimal surface voids. Also, Co depleted regions (around the WC grains) are visible, possibly caused via Co evaporation due to the extra top skin layer.

Figure 11 and Figure 12 show the SEM images of the polished vertical cross sections of the 50 W–350 J/mm³ and the 150 W–500 J/mm³ samples, respectively. In the macro view, both samples have low porosity, no cracks, and minimal large surface voids. Note the indicators within, for observations.

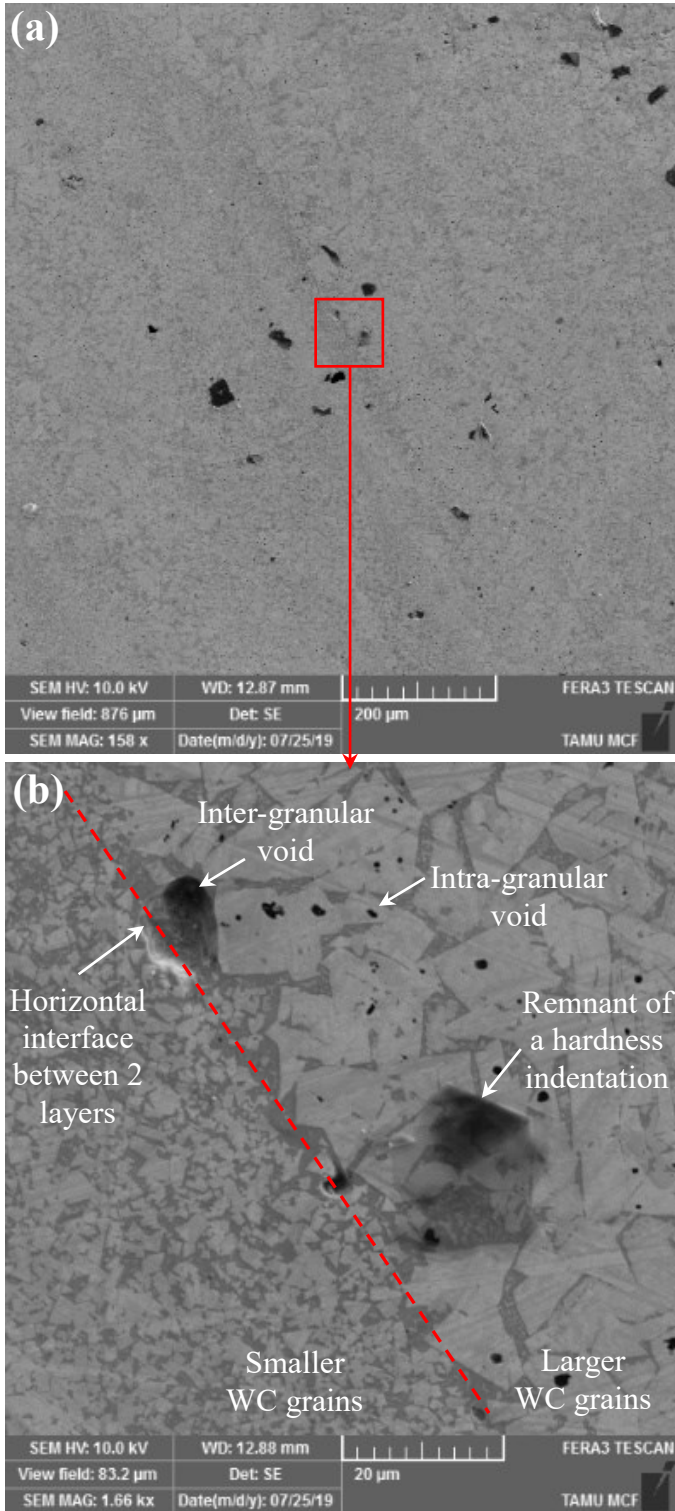


Figure 11: SEM images of 50 W–350 J/mm³ sample (vertical)

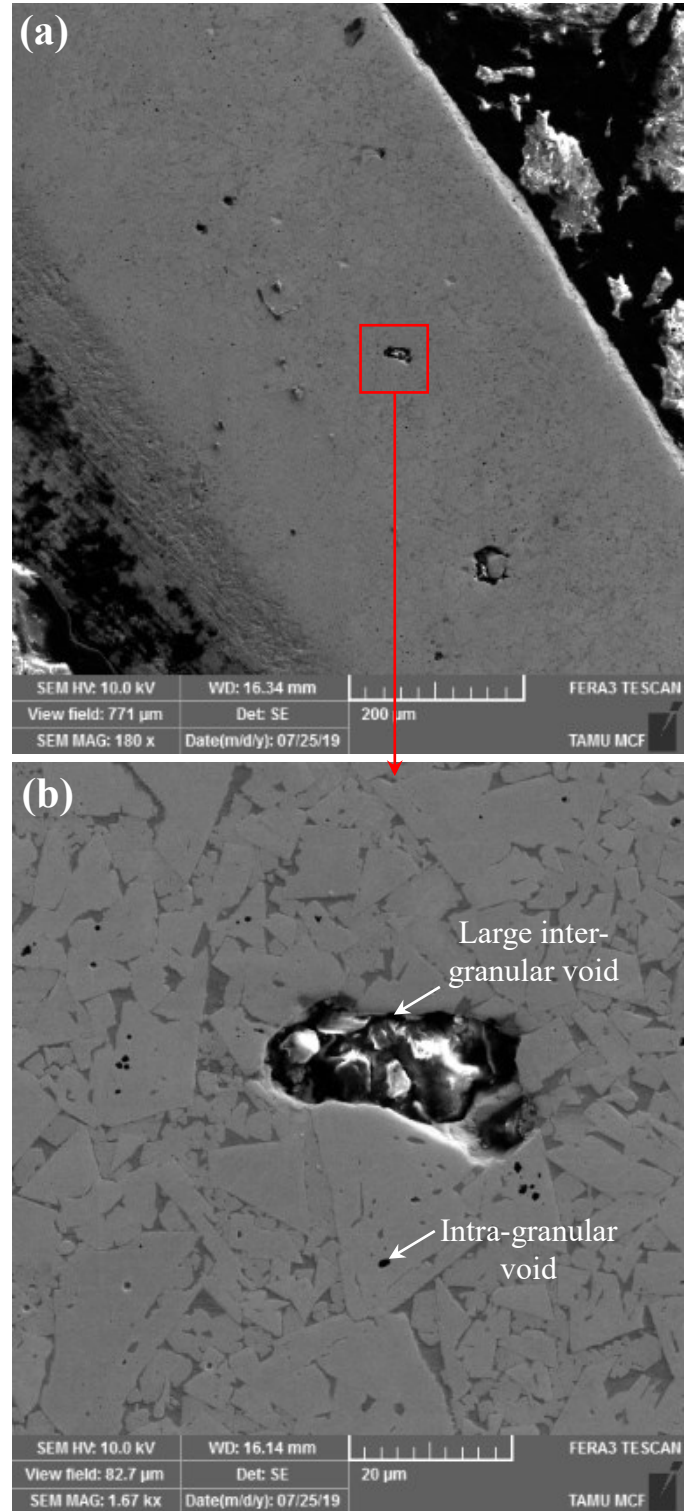


Figure 12: SEM images of 150 W–500 J/mm³ sample (vertical)

In Figure 11, the 50 W–350 J/mm³ sample displayed a distinct boundary (slanted dashed line) between two sintered powder layers, each with a significantly different average grain sizes. The smaller WC grains had an average size of 1.9 μm with a std. dev. of 0.6 μm, while the larger WC grains had an average size of 7.9 μm with a std. dev. of 2.7 μm. Being the same composition throughout, this suggests a different thermal history for each of the two layers. Additionally, with the exception of a large (possibly) inter-granular void at the boundary, all of the smaller voids (having a mean diameter of 1.4 μm with a std. dev. of 0.8 μm) seem to be within the WC grains (intra-granular), and none in the Co region. It should also be noted that all these voids were within the larger WC grains vs. the smaller WC grains; a remnant from a hardness indentation is also visible. Note that this sample is one among those (at 50 W) that had the lowest relative densities. Figure 12 depicts the 150 W–500 J/mm³ sample which recoded the second-highest density, and the highest nano-scale modulus and hardness. The grain size distribution did not show any drastic differences/trends within the region examined; the majority of the grain sizes lie within 5–20 μm. As before, a number of small intra-granular voids (on the WC grains) were visible.

3.6 Chemical Distribution

To investigate the chemical composition/distribution of the elements involved, EDS was conducted on these samples.

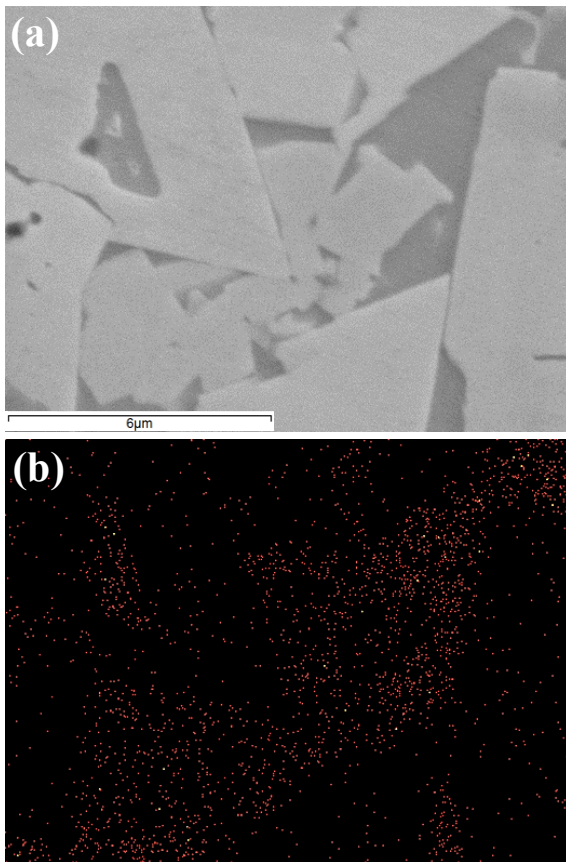


Figure 13: (a) SEM (b) Co map of 250 W–50 J/mm³ sample

Figure 13 shows the SEM image of a portion of the 250 W–350 J/mm³ sample, as well as the elemental cobalt distribution map. As expected, the Co distribution is evident in the ‘grey’ binder region between the WC grains, and seems to be fairly evenly distributed within the region. The distribution of elemental W (not shown) was densely dispersed in the regions of the WC grains, while the elemental C distribution (not shown) was sparsely dispersed within the regions of the WC grains; in some cases, the C seemed to be ‘accumulated’ closer to the WC grain boundaries, but this was not a universal trend – hence, it is merely reported as an observation.

Additionally, a number of quantitative point and area spectra were gathered for the specimens; the details of a representative sample is shown in Figure 14 and Table 3. Five specific points were probed on the WC-Co surface as detailed:

1. Spectrum 1 probe was at what seemed to be an intra-granular void (dark ‘pit’). This turned out to be a region that had the highest %C (72%) among the probed points. This is in line with prior investigations that showed C wanting to diffuse to and deposit at an open (top) or free (internal void) surface, especially at higher temperatures, often leaving behind a black/dark residue. It is interesting to find that these voids within the WC grains fabricated via SLM are in fact C sinks,

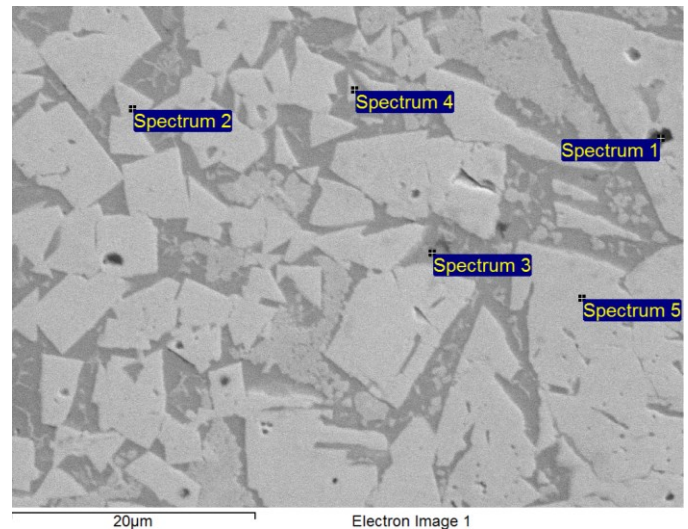


Figure 14: EDS (point spectra) of a WC-Co sample surface

Table 3: Wt. % of elements for the above point spectra

		wt% of Elements		
		C	Co	W
Spectrum	1	71.77	5.59	22.75
	2	15.95	1.19	82.14
	3	12.51	65.60	21.88
	4	12.39	30.08	57.53
	5	16.38	0.00	83.62

or conversely, the gathering together (via diffusion) of C to a spot within a WC grain could be birthing a void.

2. Spectrum 2 (and 5) probes were at the center/middle of WC grains, and quite 'far' from the grain boundaries. Consequently, the Co was mostly absent (%Co was from 0-1%) which was expected. Comprising mostly of the WC grain itself, the %W and %C were about 82% and 16% respectively. O presence was insignificant.
3. Spectrum 3 probe was at what seemed to be the 'grey' Co binder region, and as expected this point had the highest %Co (65%) among the points probed. The %W and %C were much smaller at about 21% and 12% respectively, and it is expected that the presence of WC grains very close to the point being probed, as well as any interaction of these elements with the Co binder region is what is being reflected in the numbers.
4. Spectrum 4 probe was on a small WC grain and very close to its grain boundary. In addition to significant elemental compositions of W and C as expected, there was a significant amount of Co (~30%) as well here.
5. Spectrum 5 probe was very similar to spectrum 2.

4. DISCUSSIONS

The major trends and observations from the results include:

- The lowest relative densities were observed for the samples fabricated at the lowest power (50 W); however, these had the least discoloration and competitively high hardness (both micro and nano).
- The sample relative densities were generally higher when imparting similar process volumetric energy densities via shorter exposure times.
- With the exception of the 50 W samples, densities increased with increasing volumetric energy densities.
- Micro and nano-scale hardness and modulus were comparable to traditionally made cemented carbides.
- The variation in micro-hardness, nano-hardness, and elastic modulus can be attributed to probing areas of different compositions (*i.e.*, Co vs. WC locations), large vs. small grains, composite vs. individual elements, probing voids partially/fully, etc.
- As-printed top layers showed high surface roughness and spatter spots, as well as cobalt-depleted regions around the WC grains. This was expected due to possible Co evaporation, especially due to the additional energy input via the top skin layer scan.
- Internal regions (especially for low-density samples) displayed different grain size regions separated by the layer interface. Further, small intra-granular voids were observed within larger WC grains. EDS analyses suggests that these are C deposits/sinks, bring up the question of why C diffused to a certain point/region and in a certain manner, due to or creating a void.

Based on these observations, it seems that higher energy densities (500-650 J/mm³) imparted via moderate powers (150

W) were the most suitable to maximize relative densities, with the general trend pointing to higher actual densities with increasing volumetric energies imparted. The composite micro hardness (Vickers) did not follow this trend, suggesting that it was not just the porosity (that varies inversely with density) affecting hardness, but microstructural aspects such as grain size and morphology as well. The 'homogeneity' (in grain size) of the microstructure suffered at lower power/energy density combinations leading to high porosity/voids and hence low relative densities. In contrast, a more uniform microstructural aspect (grain size) was achieved at the moderate power/higher energy density combination listed earlier, which led to less voids and higher densities.

5. CONCLUSIONS

This work served to show the successful fabrication of WC-Co bulk structures via SLM, and helped to further explore the process parameter design space as well as correlate process parameter effects on resulting properties and performance. Competitively-high density and hardness were achieved for most samples, as compared to traditionally-made WC-Co composites. Altogether, this work holds promise for the effective additive manufacturing (via SLM) of cemented carbide bulk structures that find application and will benefit customization across numerous industry sectors. Future efforts will include a directed investigation into the drastically differing grain size between sintered powder layers, its causes, formation and effects. Further, the effects of exposure times and different manners of imparting the same amount of energy will be explored, along with the probing of grain growth in the transverse direction (XY plane).

ACKNOWLEDGEMENTS

The authors would like to acknowledge the National Science Foundation (NSF) grant #1659856 for partial support of this work. The authors would also like to thank David Malawey, lab technician at Texas A&M University for his support of this work.

REFERENCES

- [1] Lu, K., 2008, "Sintering of nanoceramics," *International Materials Reviews*, 53(1), pp. 21-38.
- [2] Isakov, E., 2008, *Cutting Data for Turning of Steel*, Industrial Press.
- [3] Raihanuzzaman, R. M., Xie, Z., Hong, S. J., and Ghomashchi, R., 2014, "Powder refinement, consolidation and mechanical properties of cemented carbides — An overview," *Powder Technology*, 261(0), pp. 1-13.
- [4] Enneti, R. K., Prough, K. C., Wolfe, T. A., Klein, A., Studley, N., and Trasorras, J. L., 2018, "Sintering of WC-12%Co processed by binder jet 3D printing (BJ3DP) technology," *International Journal of Refractory Metals and Hard Materials*, 71, pp. 28-35.
- [5] Kumar, S., 2017, "Optimization of parameters for SLS of WC-Co," *Rapid Prototyping Journal*, 23(6), pp. 1202-1211.

- [6] Khmyrov, R. S., Safronov, V. A., and Gusarov, A. V., 2017, "Synthesis of Nanostructured WC-Co Hardmetal by Selective Laser Melting," *Procedia IUTAM*, 23, pp. 114-119.
- [7] Khmyrov, R. S., Safronov, V. A., and Gusarov, A. V., 2016, "Obtaining Crack-free WC-Co Alloys by Selective Laser Melting," *Physics Procedia*, 83, pp. 874-881.
- [8] Khmyrov, R. S., Shevchukov, A. P., Gusarov, A. V., and Tarasova, T. V., 2017, "Phase composition and microstructure of WC-Co alloys obtained by selective laser melting," *Mechanics & Industry*, 18(7), p. 714.
- [9] Uhlmann, E., Bergmann, A., and Gridin, W., 2015, "Investigation on Additive Manufacturing of Tungsten Carbide-cobalt by Selective Laser Melting," *Procedia CIRP*, 35, pp. 8-15.
- [10] Uhlmann, E., Bergmann, A., and Bolz, R., 2018, "Manufacturing of carbide tools by Selective Laser Melting," *Procedia Manufacturing*, 21, pp. 765-773.
- [11] Domashenkov, A., Borbély, A., and Smurov, I., 2017, "Structural modifications of WC/Co nanophased and conventional powders processed by selective laser melting," *Materials and Manufacturing Processes*, 32(1), pp. 93-100.
- [12] Chen, J., Huang, M., Fang, Z. Z., Koopman, M., Liu, W., Deng, X., Zhao, Z., Chen, S., Wu, S., Liu, J., Qi, W., and Wang, Z., 2019, "Microstructure analysis of high density WC-Co composite prepared by one step selective laser melting," *International Journal of Refractory Metals and Hard Materials*, 84, p. 104980.
- [13] Kumar, S., 2009, "Manufacturing of WC-Co moulds using SLS machine," *Journal of Materials Processing Technology*, 209(8), pp. 3840-3848.
- [14] Kumar, S., 2018, "Process chain development for additive manufacturing of cemented carbide," *Journal of Manufacturing Processes*, 34, pp. 121-130.
- [15] Cavaleiro, A. J., Fernandes, C. M., Farinha, A. R., Gestel, C. V., Jhabvala, J., Boillat, E., Senos, A. M. R., and Vieira, M. T., 2018, "The role of nanocrystalline binder metallic coating into WC after additive manufacturing," *Applied Surface Science*, 427, pp. 131-138.
- [16] Ku, N., Pittari, J. J., Kilczewski, S., and Kudzal, A., 2019, "Additive Manufacturing of Cemented Tungsten Carbide with a Cobalt-Free Alloy Binder by Selective Laser Melting for High-Hardness Applications," *JOM*, 71(4), pp. 1535-1542.
- [17] Upadhyaya, 1998, *Cemented Tungsten Carbides - Production, Properties, and Testing*, William Andrew Publishing.
- [18] HHT Hartmetall Tungsten Carbide Grades, K., K-20F and K-40UF, K-44UF and G-20." [Online]. Available: http://www.hht-hartmetall.com/en/product_range/quality.html. [Accessed: 30-Jul-2019].
- [19] <http://www.goodfellow.com/E/Tungsten-Carbide-Cobalt.html>. [Accessed: 01-Aug-2019], T. C. C.-o. c. s.-s. o. r. m. i. s. q.-G. O. A.
- [20] Huang, H., Irwan, R., and Kuriyagawa, T., 2007, "A Study on Deformation and Removal Mechanisms of Tungsten Carbide Using Nanoindentation," *Key Engineering Materials*, 329, pp. 385-390.